

# Estimation of losses in solar energy production from air pollution in China since 1960 using surface radiation data

Bart Sweerts<sup>1,2\*</sup>, Stefan Pfenninger<sup>1,3</sup>, Su Yang<sup>1,4</sup>, Doris Folini<sup>1</sup>, Bob van der Zwaan<sup>5,6,7</sup> and Martin Wild<sup>1</sup>

**China is the largest worldwide consumer of solar photovoltaic (PV) electricity, with 130 GW of installed capacity as of 2017. China's PV capacity is expected to reach at least 400 GW by 2030, to provide 10% of its primary energy. However, anthropogenic aerosol emissions and changes in cloud cover affect solar radiation in China. Here, we use observational radiation data from 119 stations across China to show that the PV potential decreased on average by 11–15% between 1960 and 2015. The relationship between observed surface radiation and emissions of sulfur dioxide and black carbon suggests that strict air pollution control measures, combined with reduced fossil fuel consumption, would allow surface radiation to increase. We find that reverting back to 1960s radiation levels in China could yield a 12–13% increase in electricity generation, equivalent to an additional 14 TWh produced with 2016 PV capacities, and 51–74 TWh with the expected 2030 capacities. The corresponding economic benefits could amount to US\$1.9 billion in 2016 and US\$4.6–6.7 billion in 2030.**

Over the past two decades, solar photovoltaic (PV) electricity generation capacity has grown exponentially worldwide. Between 2000 and 2017, worldwide installed capacity increased from 4 to 385 GW<sup>1</sup>, consistently exceeding expectations<sup>2,3</sup>. China in particular is investing heavily in PV, increasing installed capacity from less than 1 GW in 2010 to 130 GW by the end of 2017<sup>4</sup>. In 2017, China accounted for over half of global PV capacity additions<sup>5</sup>. Having surpassed the 2020 PV development target of 110 GW, China is well on track to realize its goal of reaching 400 GW of installed PV capacity by 2030, to meet its commitment to the Paris Agreement of obtaining 20% of primary energy from renewable energy sources<sup>6</sup>.

Solar radiation is often assumed to be constant over multiple years, but there is strong evidence for substantial multidecadal variations, referred to as 'global dimming and brightening'<sup>7,8</sup>. As a result of variations primarily in cloud characteristics and atmospheric aerosol concentrations, incoming radiation is scattered and absorbed, which modifies surface solar radiation<sup>9,10</sup>. In rapidly developing and heavily polluted regions, such as China, increasing anthropogenic aerosol emissions are considered a key cause of substantial dimming<sup>8</sup>. Until recently, the extent and cause of observed radiation trends in China remained unclear due to uncertainties over data quality resulting from changes in the use of instruments and observational schedules<sup>8,11,12</sup>. However, Yang et al.<sup>13</sup> homogenized a dataset covering 119 measurement stations by referencing radiation observations to more numerous sunshine duration data from nearby stations. The resulting dataset showed consistent dimming across China between 1958 and 2005 ( $-24 \pm 1 \text{ Wm}^{-2}$  ( $\pm \text{s.d.}$ )), followed by a period of brightening between 2005 and 2016

( $+7 \pm 2 \text{ Wm}^{-2}$ ). China is actively pursuing strategies to decrease air pollution, and shows signs of planning to phase out heavily polluting coal as its major energy source<sup>14</sup>. Thus, developing a deeper understanding of possible changes in surface solar radiation and their impact on a rapidly expanding PV sector is becoming increasingly important. Li et al.<sup>15</sup> analysed satellite-derived solar radiation data to find a substantial aerosol-induced reduction of solar radiation in China, with large impacts particularly over eastern China. However, the satellite data used in that study were limited to 2003–2015 and the aerosol effect was estimated using an atmospheric transfer model instead of being derived directly from measurements. Furthermore, the approach did not differentiate between anthropogenic and non-anthropogenic aerosols, which may lead to an overestimation of the effect of air pollution on surface radiation.

Here, we take a different approach by applying a PV electricity generation model, as described below, to the homogenized ground-measured radiation dataset of Yang et al.<sup>13</sup>, covering 1960–2015. We compute capacity factors (CFs), defined as the ratio between a PV panel's actual power output and maximum power output, determined under laboratory conditions (see Methods). We implicitly consider the effect of weather conditions as the simulated module's temperature increases as a function of radiation levels, which leads to lower efficiencies. Annual average CFs of commercial PV systems generally range between 0.1 and 0.35 depending on surface radiation conditions and PV panel type<sup>16</sup>. We run experiments for three different panel settings: horizontal fixed plane (HOR), fixed plane with optimal tilt (FIX) and one-axis horizontal tracking (1AX). These experiments cover PV systems ranging from residential PV panels under suboptimal tilt to more optimized utility-scale PV

<sup>1</sup>Institute for Atmospheric and Climate Science, ETH Zürich, Zürich, Switzerland. <sup>2</sup>Institute for Biodiversity and Ecosystem Dynamics, Faculty of Science, University of Amsterdam, Amsterdam, the Netherlands. <sup>3</sup>Climate Policy Group, Institute for Environmental Decisions, ETH Zürich, Zürich, Switzerland.

<sup>4</sup>National Meteorological Information Centre, China Meteorological Administration, Beijing, China. <sup>5</sup>Van 't Hoff Institute for Molecular Sciences, Faculty of Science, University of Amsterdam, Amsterdam, the Netherlands. <sup>6</sup>Energy Transition Studies, Energy Research Centre of the Netherlands, Netherlands Organisation for Applied Scientific Research (ECN-TNO), Amsterdam, the Netherlands. <sup>7</sup>School of Advanced International Studies (SAIS Europe), Johns Hopkins University, Bologna, Italy. \*e-mail: bart.sweerts@env.ethz.ch

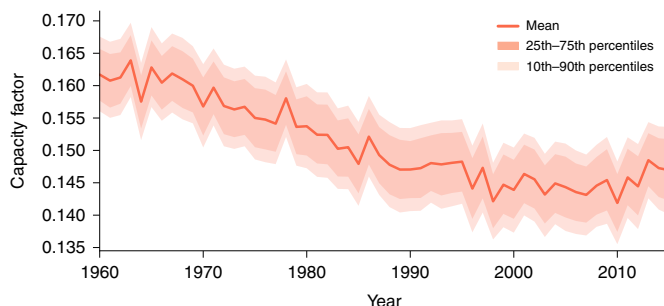


**Fig. 1 | Changes in national CFs from 1960–2015 in China.** National averages are based on CFs determined at 119 stations, which provide the essential solar radiation input data. National CFs were computed by taking the average value over all  $5^\circ \times 5^\circ$  FDM grid boxes covering China ( $n=51$ ).

installations. We compute five-year mean baseline (1961–1965) and dimmed (2011–2015) CF scenarios to analyse the impact of changes in PV resources over 50 years in China. We explore the impact of historic changes in solar radiation by analysing CF value variations for the FIX experiment between 1960 and 2015 on the national and provincial level. We investigate the influence of the HOR and 1AX panel settings on these results and discuss the possible implications of historically observed radiation changes for present and future PV electricity generation. We find that air pollution accumulation since 1960 in China has decreased solar energy potential by up to 13%, corresponding to a loss of 14 TWh of electricity in 2016.

### CFs 1960–2015

We calculate CFs at each of the 119 sites by feeding hourly solar radiation data derived from monthly mean records into the Global Solar Energy Estimator<sup>17</sup> (GSEE) and aggregating CF output to  $5^\circ \times 5^\circ$  grid cell time series using the first difference method (FDM)<sup>18</sup>. We take spatially weighed averages over relevant grid cells to compute values for each province in China, as well as a nation-wide average (see Methods for a more detailed description of the PV model setup and CF aggregation). Figure 1 shows that nation-wide averaged CFs in China decreased consistently starting in 1965. Between 1965 and 2008, mean CFs decreased by 12% from 0.162 to 0.142. After 2008, an increasing trend appears, but by 2015, CFs were still 10% lower than in 1965. Between 1960 and 2015, a negative change is observed in all months, with a strong reduction of 0.02–0.04 in the winter months (November to February), and a weaker reduction of 0.01–0.02 in the summer months (June to August) (Supplementary Fig. 1). Intra-annual variation of CFs increases through time (Supplementary Fig. 2), potentially exacerbating intermittency issues inherent to the use of solar energy. The strong reduction in CFs observed in winter may be due to higher residential aerosol emissions as a result of biomass and fossil fuel-powered heating<sup>19,20</sup>.

The five-year average baseline scenario (1961–1965) shows a spatial pattern of higher CFs in the northern and north-western provinces, with a maximum of 0.22 in Tibet, and lower values in the south-eastern provinces, with a minimum of 0.09 in Chongqing (Fig. 2a). South-eastern provinces are characterized by, on average, around 50% lower CFs than north-western provinces. Higher cloud cover over the humid subtropical south-eastern provinces than over the arid highlands of the north-western provinces is the primary cause for the difference in the geographical distribution of solar radiation. Additionally, regions with high altitudes, such as the Tibetan Plateau, receive more surface solar radiation as a result of a smaller total air column (as shown for our dataset in Supplementary Fig. 3)<sup>21</sup>.

The overall distribution of CFs under dimmed (2011–2015) conditions is similar to that of the baseline scenario (Fig. 2b). However,

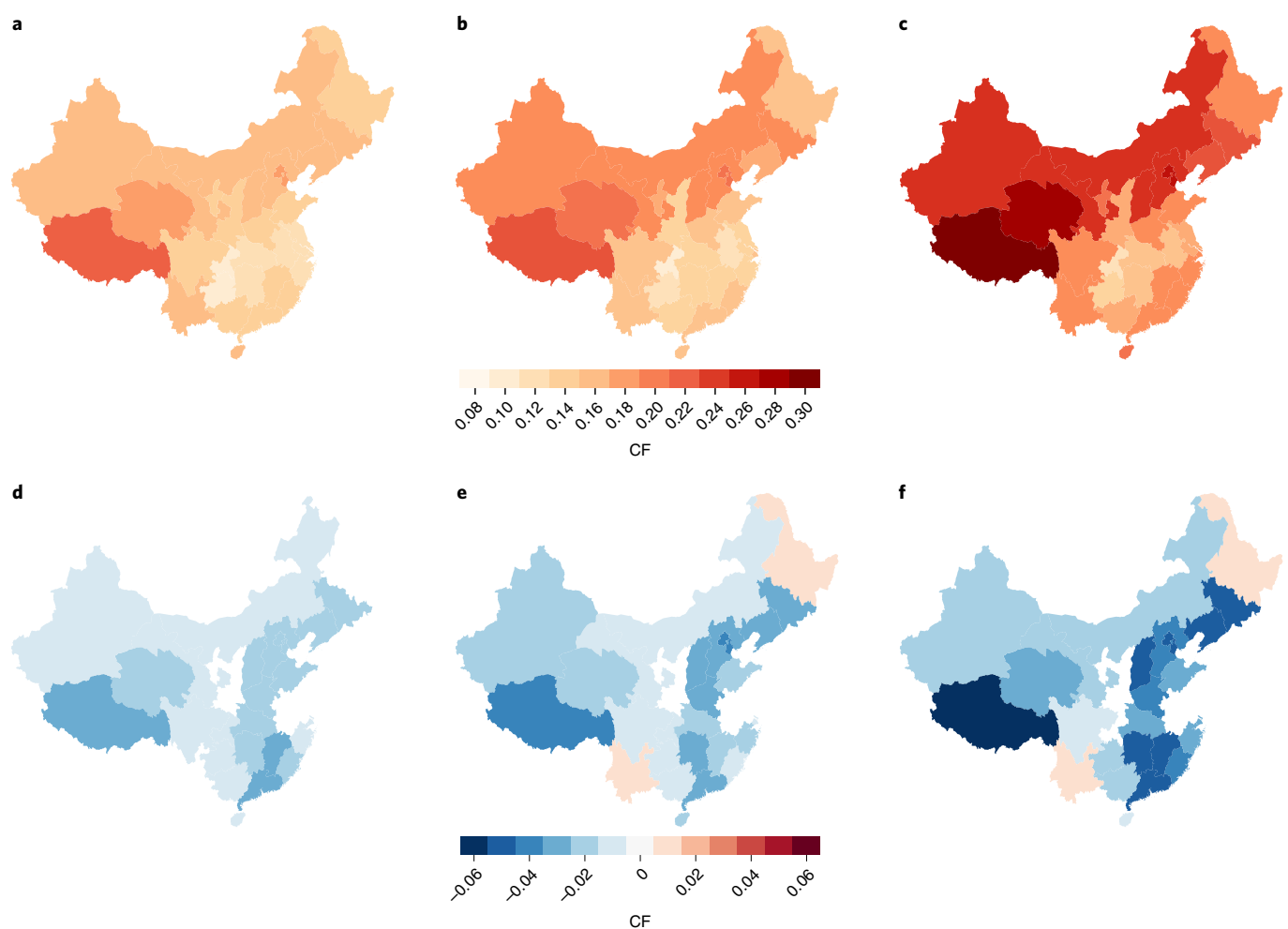
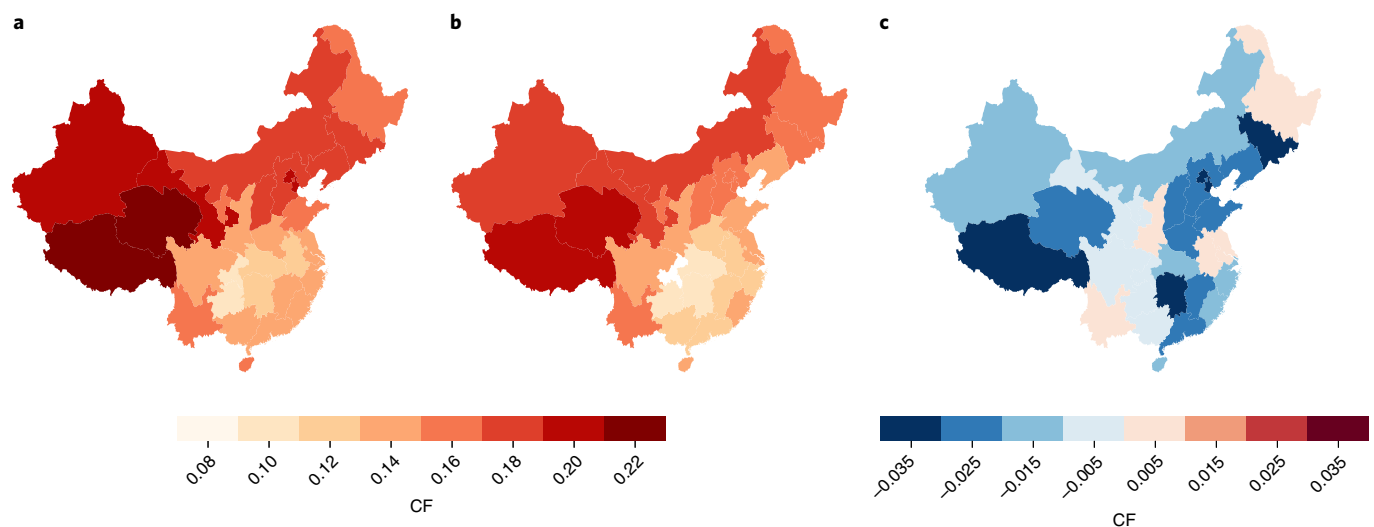
CFs are lower in 27 out of 31 provinces, with the largest absolute change observed in the heavily polluted eastern and southern provinces, as well as in Tibet and Qinghai (Fig. 2c). The large change observed in Tibet and Qinghai—two provinces largely located on the Tibetan Plateau—is unexpected, as it is one of the least densely populated regions of China and contains limited industrial areas. However, as a result of the logarithmic relationship between aerosol optical depth (AOD) and aerosol radiative forcing<sup>10</sup>, regions with low background AOD, such as the Tibetan Plateau, may experience large changes in radiation due to relatively small changes in atmospheric aerosol concentrations. A comprehensive study analysing observations, reanalyses and global climate model ensemble simulations found that large-scale transported as well as locally emitted aerosols are a plausible cause for radiation reductions observed between 1960 and 2005 on the Tibetan Plateau<sup>22</sup>. Also, the absolute radiative effect of increasing AOD is proportional to the initial radiation levels. We find that percentage changes in CF between 1960 and 2015 are in fact largest in the densely populated and heavily polluted south-eastern regions (Supplementary Fig. 4). The estimated changes increase the difference between the high-radiation north-western and low-radiation south-eastern provinces. Compared with the baseline, provincial CFs decreased by 20–28% in the five most heavily affected provinces. Four provinces show a small positive change (+0 to +4%). Robust linear regression trends computed for CF time series between 1960 and 2015 were found to be significant in all provinces with a negative change, but only in one out of four provinces with a positive change (Supplementary Fig. 5).

### Sensitivity of results to panel settings

Small-scale distributed PV systems are usually mounted at a fixed angle. The optimum mounting angle changes with latitude, but for residential applications, the angle is often constrained by the rooftop angle or building regulations. PV systems with one- or two-axis tracking, which more optimally utilize direct radiation by minimizing the incidence angle of sunlight relative to the panel normal, are more frequently used in utility-scale solar farms. By the end of 2016, small-scale distributed PV accounted for 13% of installed PV capacity in China<sup>23</sup>. This share grew substantially in 2017, when distributed capacity additions rose to 19 GW, accounting for 38% of newly installed PV capacity<sup>24</sup>. It is expected that the share of distributed PV will continue to rise between now and 2030<sup>13</sup>.

Optimally tilted fixed-angle and tracking systems yield the largest efficiency gains in high-radiation areas in western and northern China (Fig. 3a). We find that, for provinces in these regions, the FIX and 1AX experiments result in 13–21% and 47–54% higher yields, respectively, compared with HOR. In contrast, yields in southern and eastern China show no significant increase for FIX and a 14–25% increase for 1AX compared with HOR, due to a higher share of diffuse radiation in these regions. As a result, a large share of Chinese utility-scale solar parks is located in the high-radiation north-western provinces, such as Xinjiang, Qinghai and Gansu, while distributed PV is more evenly distributed across China<sup>23</sup>.

Absorption and scattering of solar radiation by aerosols and clouds decrease the fraction of direct radiation and increase the fraction of diffuse radiation<sup>25</sup> (as shown for our dataset in Supplementary Fig. 6). As the efficiency gains of PV panels equipped with tracking systems result from more effective use of direct radiation, they are more strongly affected (in absolute terms and percentage wise) by decreasing solar radiation resources than fixed panels are. Compared with 1961–1965 means, average CFs for 2011–2015 are 9% (HOR), 11% (FIX) and 15% (1AX) lower (Fig. 3b). The observed decrease in CFs for FIX is, on average, roughly half (−11%) as large as the benefit of switching from FIX to 1AX (+24%) under dimmed radiation conditions. The pattern of change is similar for all three experiments, with two exceptions (Fig. 3b). First, in the most north-western province of Xinjiang,



the change relative to other provinces is less pronounced in 1AX than in FIX. Second, the southern Yunnan province shows a positive change in FIX and 1AX, but a negative change in HOR. Furthermore, compared with FIX, the 1AX experiment shows non-significant linear regression trends in two additional provinces: Shaanxi and Anhui.

### Impact on energy sector

The reduction of solar radiation resources observed over the past 50 years has a significant impact on the present-day production of solar electricity in China. This impact will increase depending on how China's PV sector develops in the future. We compare electricity generation under 1961–1965 (baseline) and 2011–2015 (dimmed) radiation levels for installed capacity at the end of 2016, as well as different capacity scenarios for 2030. The four capacity scenarios for 2030 cover high (422 GW) and low (300 GW) penetration of PV with high (45%) and low (20%) shares of distributed PV. Electricity production is computed on the provincial scale. We assume FIX CFs for distributed and 1AX CFs for utility-scale PV installations. For provinces where no significant linear regression trends were found for 1AX or FIX, CFs are kept constant at baseline levels.

The difference in electricity generation over the whole of China, comparing the baseline and dimmed radiation levels, and with 2016 installed PV capacities, are estimated at 14 TWh yr<sup>-1</sup>, or 12% of total 2016 PV electricity generation (Table 1). Under 2016 Chinese feed-in tariffs (FITs) of US\$0.14 kWh<sup>-1</sup>, this translates to US\$1.9 billion yr<sup>-1</sup> (based on 2016 US\$) of FIT revenue gains for plant operators if the radiation levels of the 1960s could be reached again. For the 2030 capacity scenarios, potential electricity gains with 1960s radiation levels range from 51–74 TWh yr<sup>-1</sup>, or 12–13% of total PV electricity generation. Under the assumption that FITs are phased out by 2030, and that the price of electricity remains constant at the 2016 level of US\$0.09 kWh<sup>-1</sup>, these PV electricity gains would result in cost savings of US\$4.6–6.7 billion yr<sup>-1</sup> (based on 2016 US\$). The two capacity scenarios with higher shares of distributed PV result in only 3.5% lower potential gains compared with utility-dominated scenarios, despite the significantly larger average CF reductions estimated for 1AX. This is caused by north-western provinces, which contain a large proportion of utility-scale PV in the 2030 capacity scenarios, showing a relatively small difference between FIX and 1AX in terms of historic CF.

With 2016 installed capacity, over half of the difference in electricity generation between the baseline and dimmed radiation scenario occurs in five provinces. These are located in high-radiation northern China and densely populated eastern China (Supplementary Fig. 7). The largest differences are observed in provinces with high installed capacity and large CF changes, such as Gansu, Xinjiang and Hebei. Tibet, Jilin and Liaoning are among the provinces showing the largest decreases in CFs, but differences in electricity generation are minor as a result of low installed capacities. For the 2030 capacity scenarios with low shares of distributed PV, the differences between historic and dimmed radiation levels are highest in the high-radiation northern and western provinces (Supplementary Fig. 8). In comparison, the scenarios with higher shares of distributed PV show larger differences in low-radiation, high-population provinces with large shares of distributed PV, such as Hebei, Shandong and Guangdong.

### Aerosol emissions and CFs

To what extent observed dimming should be attributed to anthropogenic aerosol emissions, natural cloud variability or naturally occurring aerosols such as dust or salt particles remains debated<sup>8</sup>. The strong correlation and absence of obvious alternative explanations suggest that the majority of observed dimming in China is due to anthropogenic aerosol emissions. Aerosol emissions have increased rapidly in China along with its industrialization since the early 1950s<sup>26–28</sup>. Sulfur dioxide (SO<sub>2</sub>) and black carbon—a major

**Table 1 | Potential electricity generation benefits, assuming that returning to 1960s radiation levels is possible**

Year	Total PV capacity (GW)	Utility-scale PV (GW)	Distributed PV (GW)	Total electricity yield (TWh yr <sup>-1</sup> ) <sup>a</sup>	Potential electricity gain (TWh yr <sup>-1</sup> )
2016	77	67 (87%)	10 (13%)	118	14
2030	300	240 (80%)	60 (20%)	446	53
2030	300	164 (55%)	136 (45%)	405	51
2030	422	338 (80%)	84 (20%)	627	74
2030	422	230 (55%)	192 (45%)	569	72

<sup>a</sup>PV electricity generation with 2011–2015 (dimmed) CFs.

component of fine particulate matter (PM<sub>2.5</sub>)—serve as precursors to atmospheric aerosol species that are most important for the absorption and scattering of solar radiation in China.

Folini and Wild<sup>29</sup> conducted transient sensitivity experiments with a global climate model with sophisticated treatment of aerosol and cloud microphysics, finding that between 1950 and 2000, SO<sub>2</sub> and the combination of black carbon and organic carbon emissions caused two-thirds and one-third of observed dimming in eastern China, respectively. During the dimming period in China between 1955 and 2000, cloud amounts decreased simultaneously with decreasing surface radiation<sup>30,31</sup>, suggesting that clouds may not have contributed to the dimming, leaving aerosols as the most likely cause. Furthermore, ref. <sup>13</sup> found that dimming in China is at least as strong or stronger under clear-sky conditions as it is under all-sky conditions. Dimming under clear-sky conditions occurs primarily due to increasing aerosol concentrations, and aerosol-induced dimming is thought to persist under cloudy conditions. Thus, these findings support the hypothesis that aerosols, rather than clouds, are the primary cause for observed dimming in China. This is further supported by Norris and Wild<sup>32</sup>, who isolated the radiative effect of cloud cover anomalies to find that changes in cloud cover made a negligible contribution to dimming in China between 1971 and 1989.

We find a strong correlation between national annual mean CFs estimated in the present study and SO<sub>2</sub> and black carbon emissions between 1960 and 2015 as provided by Peking University emission inventories (<http://inventory.pku.edu.cn/home.html>, Fig. 4a and Supplementary Fig. 9). On the basis of this, and given evidence from previous work, we find it plausible that reducing aerosol emissions to historic 1960s levels will result in a return of ground solar radiation to historically observed levels.

### Policy relevance and conclusions

Between 1996 and 2010, an estimated 91% of SO<sub>2</sub> emissions in China originated from the combustion of coal—mostly in industry and power generation<sup>33</sup>. For the same period, the majority of black carbon was emitted as a result of residential and industrial coal (41%) and biomass (33%) consumption<sup>33</sup>. Since the early 1990s, anthropogenic aerosol emissions of black carbon have decreased and emissions of SO<sub>2</sub> have increased at a substantially lower rate than coal consumption (Fig. 4b). Aerosol emission factors (that is, the amount of aerosols emitted per unit of fuel burned) of SO<sub>2</sub> and black carbon have decreased in China as a result of national air pollution control policies and demographic changes<sup>34,35</sup>. Black carbon emissions from residential biomass burning declined as a result of a demographic shift towards a more urbanized population, starting in the 1990s. The 1996 Coal Law reduced industrial black carbon emissions by limiting beehive coke ovens, and initiated a transition towards more efficient coal power stations<sup>28</sup> (Fig. 4b, policy 1). The first policies promoting the desulfurization of coal power plants

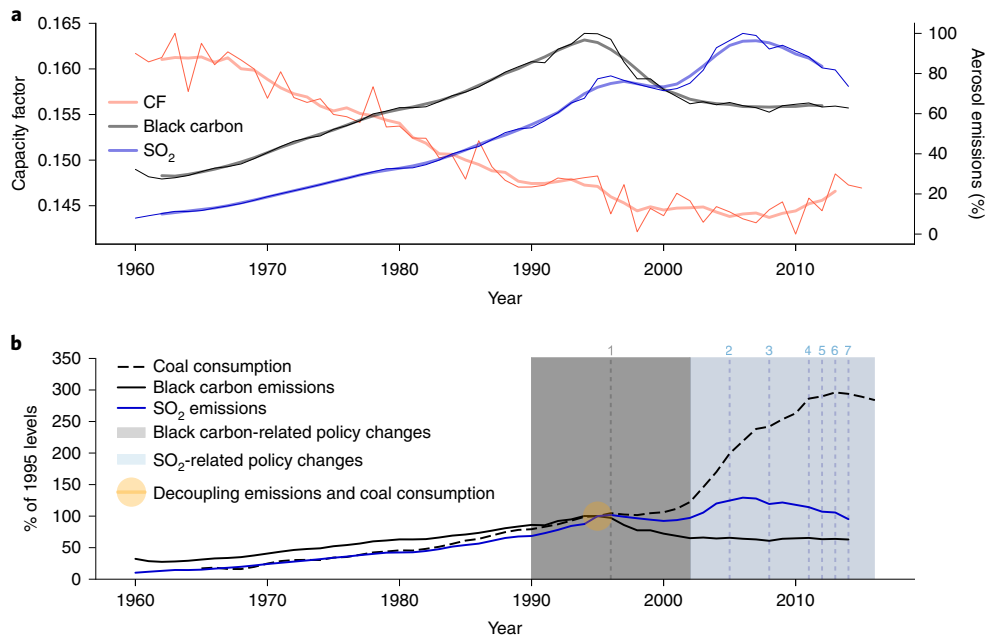


**Fig. 4 | Aerosol emissions, estimated CFs and air pollution policy regulations from 1960–2015.** **a**, Historic (1960–2015) FIX CFs (red lines), SO<sub>2</sub> emissions (blue lines) and black carbon emissions (black lines) in China as a percentage of peak emissions in 1994 and 2005, respectively. Thin lines show annual values, while thick lines show five-year moving mean values. **b**, Historic (1960–2015) SO<sub>2</sub> (blue line) and black carbon (black line) emissions and coal consumption (dashed black line). Values are shown relative to 1995 (highlighted in orange), since from that year onwards aerosol emissions decoupled from coal consumption (see Supplementary Fig. 10). Shaded areas indicate periods of decreasing aerosol emission factors for SO<sub>2</sub> (blue) and black carbon (grey) as a result of regulations and demographic changes. Numbered vertical lines indicate years of adoption for national aerosol emission policies: (1) phase-out of beehive coke ovens; (2) desulfurization techniques in power plants; (3) stricter control of desulfurization techniques in power plants; (4) shift of coal to more gas and renewable energies; (5) new emission standards for thermal power plants; (6) 'Action Plan for Air Pollution and Control' introduces strict air pollution standards and emission goals until 2030; and (7) phasing out small-scale coal-fired boilers; use of low-sulfur coal; and cap on coal consumption. SO<sub>2</sub> and black carbon emissions were taken from Peking University emission inventories (<http://inventory.pku.edu.cn/home.html>, see Supplementary Note 2). Regulations and demographic changes are described in Supplementary Table 2. Coal consumption data were taken from the British Petroleum energy economics charting tool<sup>33</sup>.

were implemented in 2005/2006, resulting in a 10% reduction in SO<sub>2</sub> emissions between 2006 and 2010 (Fig. 4b, policy 2). The 12<sup>th</sup> five-year plan (2011–2015) introduced a shift towards low-sulfur energy generation (Fig. 4b, policies 3–5), which, combined with stricter control on compliance with desulfurization regulations, further reduced SO<sub>2</sub> emissions by 18% despite rapidly rising coal consumption<sup>36</sup>. Transport emissions have increased over the past two decades to offset some emissions reductions from cleaning up stationary sources. However, in the medium term, tighter emissions standards and electrification of transport are expected to reduce these emissions as well<sup>37</sup>.

Large concerns over the negative health effects of severe air pollution<sup>37,38</sup>, including from secondary aerosol precursors<sup>39</sup>, continue to push China towards policies that aim to reduce aerosol emissions and limit coal consumption. The 13<sup>th</sup> five-year plan (2016–2020) calls for a reduction of SO<sub>2</sub> emissions by 15% compared with 2015 levels. In 2013, China implemented the 'Action Plan of Air Pollution and Control', setting stricter than ever targets for the reduction of emissions of pollutants, including reductions of SO<sub>2</sub> and PM<sub>2.5</sub> by at least 53 and 57%, respectively, by 2030 compared with 2012<sup>40</sup> (Fig. 4b, policy 6). In addition to further deployment of emission reduction technologies, China aims to cap and reduce coal consumption, as evidenced by declining coal consumption over the past five years (Fig. 4b, policy 7). Given the success of previous and current air pollution control policies, we find it plausible that aerosol emissions will continue to decline between now and 2030, with an increase in solar PV electricity generation potential as a result. While it should be technically achievable to return to near-zero

emissions in China, and China is committed to climate change mitigation, the timeline and cost of further emissions reductions in the near to medium term remain uncertain.

Reducing air pollution to 1960s levels would result in an 'electricity bonus' of 14 TWh yr<sup>-1</sup> of additional PV generation, given the installed PV capacity in 2016, and between 51 and 74 TWh yr<sup>-1</sup> in 2030. The estimated total welfare losses due to air pollution in China are estimated by the World Health Organization at USD\$1.6 trillion in 2013<sup>41</sup>, which of course far exceeds the economic value of these estimated PV electricity gains. Thus, our findings should be interpreted as a possible co-benefit of air pollution control in China. As a result of the growing share of PV in the electricity mix, potential gains could increase to close to 1% of total electricity production in 2030. Since, as discussed above, it is likely that a significant part of dimming over China is caused by aerosol absorption rather than scattering, cleanup of this pollution may not substantially increase surface temperatures in China, since a reduction of absorbing aerosol, in contrast with scattering aerosol, leads to a cooling rather than a warming. We consider seasonal weather variations implicitly by including the impact of radiation levels on module temperature and efficiency. Future work could include temperatures explicitly or consider possible correlations between dimming and low wind speed, which could be relevant for the stability of the overall power, given increasing shares of both wind and solar power. The cost of PV panels now makes up only 30% of total costs for utility-scale PV installations, with the remainder of costs coming from area-related balance-of-system costs such as labour for installation, financing and customer acquisition<sup>42</sup>. As balance-of-system costs

do not decrease nearly as quickly as panel costs, efficiency gains will probably become increasingly important in the reduction of overall system costs. If a 12–13% increase in PV electricity production is possible by eliminating most air pollution by 2030, it would exceed the technology-driven efficiency improvements for crystalline-silicon PV panels of 8–10% achieved between 2005 and 2017<sup>43,44</sup>.

## Methods

**GSEE model description.** We use the open-source GSEE model<sup>17</sup> on the [www.renewables.ninja](http://www.renewables.ninja) web platform and available on [www.github.com/renewables-ninja/gsee](https://github.com/renewables-ninja/gsee) to estimate CFs for hourly radiation values derived from monthly mean global horizontal radiation records from 119 measurement stations in China. As input, the model takes hourly direct and diffuse horizontal radiation ( $\text{kW m}^{-2}$ ), which is obtained as described in the sections below. The ambient temperature is set to the default value of 20°C to isolate the effect of changes in radiation levels on PV electricity generation potential. The modules' temperature increases from the default value as a function of incident irradiance at 0.035 °C  $\text{W}^{-1} \text{m}^{-2}$ . Energy input is then computed using in-plane irradiance and temperature-dependent efficiency curves (for a more detailed description of the PV model and the underlying assumptions, see Supplementary Note 3 and Pfenninger and Staffel<sup>17</sup>). Three different settings for PV panel angles are used: (1) HOR; (2) FIX; and (3) 1AX. Direct and diffuse panel irradiance is calculated depending on panel settings, from which electricity generation is computed. We assume 10% loss from inverter and other system components based on data on these losses being 10 ± 4% across 1,029 sites in Europe<sup>17</sup>. We always set installed capacity to 1 kW, which allows for easy conversion of output ( $\text{PV}_{\text{out}}$ ) to CF, defined as the ratio between a panel's actual energy output and its maximum output under optimum test conditions (specified as 1,000  $\text{W m}^{-2}$  at the AM1.5 spectrum and a cell temperature of 25 °C).

**Solar radiation data.** We use monthly global horizontal radiation data from 119 measurement stations in China covering 1960–2016. There have been considerable uncertainties regarding the quality of measured radiation data in China<sup>13,45</sup>. The radiation data series used in this study are taken from Yang et al.<sup>13</sup>, who homogenized the dataset using neighbouring surface sunshine duration measurements, resulting in changes to 60 out of 119 stations originally provided by the Chinese Meteorological Agency (for a detailed description of the radiation data, see Supplementary Note 1). The dataset covers all provinces, with a higher density of measurement stations in densely populated eastern China, as shown in Supplementary Fig. 11. The number of stations increased slowly until 1989, when the Chinese Meteorological Administration adopted a new measurement system, and some stations were shut down or replaced while other stations were opened in the following years. Most inhomogeneity issues were caused by instrument or observation schedule changes. The homogenization process as described in Yang et al.<sup>13</sup> mostly focuses on these transition points.

**Monthly to hourly radiation and diffuse fraction.** Direct and diffuse radiation as inputs for GSEE are computed in three steps, following the approach described previously<sup>46</sup>: (1) we convert monthly mean radiation values to daily means; (2) we construct hourly means from the daily data; and (3) we compute the hourly diffuse irradiance fraction. For the first step, daily values are estimated on the basis of monthly probability density functions (PDFs) of daily radiation measurements from 12 measurement stations in China available from the World Radiation Data Centre (WRDC) (see Supplementary Table 1). For each of the 119 stations reporting monthly means used in this study, the daily values were computed using a PDF constructed from the nearest WRDC reference station. Observations are aggregated per month over the measurement time period (ranging between 12 and 28 years across stations). From these aggregates, PDFs are constructed. Supplementary Fig. 12 shows an example output of 12 monthly PDFs computed for Beijing. The computed PDFs generally resemble a normal distribution with a tail to the left extending up to roughly 0  $\text{kW m}^{-2}$ . For each day in a month, the daily radiation value can then be computed from the observed monthly mean (RM) using:

$$r_{m,d} = r \sim f(r)_m \cdot \frac{\text{RM}}{\mu_{f_m}}$$

where  $r \sim f(r)_m$  is a random draw from the PDF of the relevant month,  $m$ , and  $\frac{\text{RM}}{\mu_{f_m}}$  is the fraction between the observed monthly mean and the PDF's mean.

The WRDC station used to estimate daily values from monthly means at a given location is chosen based on spatial proximity. For the second step, hourly radiation values are constructed by distributing daily radiation across the hours of the day using a sinus function:

$$r_{d,h} = \max \left( 0, \sin \left( \left( \frac{\pi}{h_{\text{set},d} - h_{\text{rise},d}} \right) \cdot (h - h_{\text{rise},d}) \right) \cdot \frac{24\pi \cdot r_d}{2 \cdot (h_{\text{set},d} - h_{\text{rise},d})} \right)$$

where  $h_{\text{rise},d}$ ,  $h_{\text{set},d}$  are the sunrise and sunset hour, and  $h$  is the hour of the day. Sunset and sunrise times were calculated using the astronomical computation library PyEphem. For the third step, the diffuse fraction (that is, the percentage of the global radiation that is scattered in the atmosphere through clouds and aerosols) is calculated. It is estimated with the Boland–Ridley–Lauret model (for details on calculations, see ref. <sup>47</sup>). The Boland–Ridley–Lauret model uses an hourly clearness index, which is estimated as the fraction of observed global horizontal radiation and top of atmosphere radiation.

**FDM temporal trend analysis.** We use the FDM to compute temporal CF trends across China. FDM was developed to reduce uncertainties caused by inhomogeneous and incomplete records, as well as different series lengths, while permitting the resulting reference series to contain as much of the observed data as possible<sup>18</sup>. For each measurement station, a first difference series is computed using:

$$\delta CF_t = CF_t - CF_{t-1}$$

where  $CF_t$  is the CF at time  $t$ . The difference series are aggregated to  $5^\circ \times 5^\circ$  grid boxes by taking the mean difference for each year for all stations within each grid box. To obtain absolute values, the mean value of a reference period (in our case, the first set of observations in each grid box) is added to the aggregated difference series. Provincial-level CFs are then computed by taking the weighted mean of the grid boxes that cover (part of) the province. Weights are assigned to each grid box value by the fraction of the province covered by that grid box. Trend patterns for solar radiation in China are found to be spatially coherent (as shown, for example, by Yang et al.<sup>13</sup>), which supports the representativeness of our regional disaggregation.

## Data availability

A subset of the data used in this paper is available from the Chinese Meteorological Administration data portal (<https://data.cma.cn>). The data that support the plots within this paper and other findings of this study are available from the corresponding author upon reasonable request.

## Code availability

The GSEE PV simulation model is available at <https://github.com/renewables-ninja/gsee>. The code used to produce CFs from the homogenized dataset is available from the corresponding author on reasonable request.

Received: 24 September 2018; Accepted: 14 May 2019;

Published online: 08 July 2019

## References

- Renewable Energy Statistics 2018 (IRENA, 2018).
- Creutzig, F. et al. The underestimated potential of solar energy to mitigate climate change. *Nat. Energy* **2**, 17140 (2017).
- Haegel, N. M. et al. Terawatt-scale photovoltaics: trajectories and challenges. *Science* **356**, 141–143 (2017).
- National Electric Power Industry Statistics (NEA, 2017).
- Renewables 2017: Analysis and Forecasts to 2022—Executive Summary (IEA, 2017).
- China Wind, Solar and Bioenergy Roadmap 2050 (CNREC, 2014).
- Wild, M. et al. From dimming to brightening: decadal changes in solar radiation at Earth's surface. *Science* **308**, 847–850 (2005).
- Wild, M. Decadal changes in radiative fluxes at land and ocean surfaces and their relevance for global warming. *Wiley Interdiscip. Rev. Clim. Change* **7**, 91–107 (2016).
- Streets, D. G., Wu, Y. & Chin, M. Two-decadal aerosol trends as a likely explanation of the global dimming/brightening transition. *Geophys. Res. Lett.* **33**, L15806 (2006).
- Wild, M. et al. Global dimming and brightening: an update beyond 2000. *J. Geophys. Res. Atmos.* **114**, D00D13 (2009).
- Shi, G. Y. et al. Data quality assessment and the long-term trend of ground solar radiation in China. *J. Appl. Meteorol. Climatol.* **47**, 1006–1016 (2008).
- Tang, W. J., Yang, K., Qin, J., Cheng, C. C. K. & He, J. Solar radiation trend across China in recent decades: a revisit with quality-controlled data. *Atmos. Chem. Phys.* **11**, 393–406 (2011).
- Yang, S., Wang, X. L. & Wind, M. Homogenization and trend analysis of 1958–2016 in situ surface solar radiation records in China. *J. Clim.* **31**, 4529–4541 (2018).
- Qi, Y., Stern, N., Wu, T., Lu, J. & Green, F. China's post-coal growth. *Nat. Geosci.* **9**, 564–566 (2016).
- Li, X., Wagner, F., Peng, W., Yang, J. & Mauzerall, D. L. Reduction of solar photovoltaic resources due to air pollution in China. *Proc. Natl. Acad. Sci. USA* **114**, 11867–11872 (2017).
- Renewables 2017: Global Status Report (REN21, 2017).

17. Pfenninger, S. & Staffell, I. Long-term patterns of European PV output using 30 years of validated hourly reanalysis and satellite data. *Energy* **114**, 1251–1265 (2016).
18. Peterson, T. C., Karl, T. R., Jamason, P. F., Knight, R. & Easterling, D. R. First difference method: maximizing station density for the calculation of long-term global temperature change. *J. Geophys. Res. Atmos.* **103**, 25967–25974 (1998).
19. Xiao, Q., Ma, Z., Li, S. & Liu, Y. The impact of winter heating on air pollution in China. *PLoS ONE* **10**, e0117311 (2015).
20. Liu, J. et al. Air pollutant emissions from Chinese households: a major and underappreciated ambient pollution source. *Proc. Natl Acad. Sci. USA* **113**, 7756–7761 (2016).
21. Blumthaler, M., Ambach, W. & Ellinger, R. Increase in solar UV radiation with altitude. *J. Photochem. Photobiol. B* **39**, 130–134 (1997).
22. You, Q. et al. Decadal variation of surface solar radiation in the Tibetan Plateau from observations, reanalysis and model simulations. *Clim. Dynam.* **40**, 2073–2086 (2013).
23. *Photovoltaic Power Statistics* (NEA, 2016).
24. *Proc. Introducing the 2017 Energy Situation* (NEA, 2018); [http://www.nea.gov.cn/2018-01/24/c\\_136921015.htm](http://www.nea.gov.cn/2018-01/24/c_136921015.htm)
25. Kvælevåg, M. M. & Myhre, G. Human impact on direct and diffuse solar radiation during the industrial era. *J. Clim.* **20**, 4874–4883 (2007).
26. Bond, T. C. et al. Historical emissions of black and organic carbon aerosols from energy-related combustion, 1850–2000. *Global Biogeochem. Cycles* **21**, GB2018 (2007).
27. Smith, S. J. et al. Anthropogenic sulfur dioxide emissions: 1850–2005. *Atmos. Chem. Phys.* **11**, 1101–1116 (2011).
28. Wang, R. et al. Black carbon emissions in China from 1949 to 2050. *Environ. Sci. Technol.* **46**, 7595–7603 (2012).
29. Folini, D. & Wild, M. The effect of aerosols and sea surface temperature on China's climate in the late twentieth century from ensembles of global climate simulations. *J. Geophys. Res.* **120**, 2261–2279 (2015).
30. Liu, B., Xu, M., Henderson, M., Qi, Y. & Li, Y. Taking China's temperature: daily range, warming trends, and regional variations, 1955–2000. *J. Clim.* **17**, 4453–4462 (2004).
31. Qian, Y., Kaiser, D. P., Leung, L. R. & Xu, M. More frequent cloud-free sky and less surface solar radiation in China from 1955 to 2000. *Geophys. Res. Lett.* **33**, L01812 (2006).
32. Norris, J. R. & Wild, M. Trends in aerosol radiative effects over China and Japan inferred from observed cloud cover, solar 'dimming' and solar 'brightening'. *J. Geophys. Res. Atmos.* **114**, D00D15 (2009).
33. Lu, Z., Zhang, Q. & Streets, D. G. Sulfur dioxide and primary carbonaceous aerosol emissions in China and India, 1996–2010. *Atmos. Chem. Phys.* **11**, 9839–9864 (2011).
34. Wang, R. et al. Trend in global black carbon emissions from 1960 to 2007. *Environ. Sci. Technol.* **48**, 6780–6787 (2014).
35. Li, C. et al. India is overtaking China as the world's largest emitter of anthropogenic sulfur dioxide. *Sci. Rep.* **7**, 14304 (2017).
36. Wu, Y. et al. On-road vehicle emissions and their control in China: a review and outlook. *Sci. Total Environ.* **574**, 332–349 (2017).
37. Yang, G. et al. Rapid health transition in China, 1990–2010: findings from the Global Burden of Disease Study 2010. *Lancet* **381**, 1987–1995 (2013).
38. Lelieveld, J., Evans, J. S., Fnais, M., Giannadaki, D. & Pozzer, A. The contribution of outdoor air pollution sources to premature mortality on a global scale. *Nature* **525**, 367–371 (2015).
39. Huang, R. J. et al. High secondary aerosol contribution to particulate pollution during haze events in China. *Nature* **514**, 218–222 (2015).
40. *Performance Evaluation on the Action Plan of Air Pollution Prevention and Control and Regional Coordination Mechanism* (CCICED, 2014).
41. *The Cost of Air Pollution Strengthening the Economic Case for Action* (World Bank, 2016).
42. Lewis, N. S. Research opportunities to advance solar energy utilization. *Science* **351**, aad1920 (2016).
43. Green, M. A., Emery, K., King, D. L., Hisikawa, Y. & Warta, W. Solar cell efficiency tables (version 27). *Prog. Photovolt.* **14**, 45–51 (2006).
44. Green, M. A. et al. Solar cell efficiency tables (version 51). *Prog. Photovolt. Res. Appl.* **26**, 3–12 (2018).
45. Xia, X. A closer looking at dimming and brightening in China during 1961–2005. *Ann. Geophys.* **28**, 1121–1132 (2010).
46. Müller, J., Folini, D., Wild, M. & Pfenninger, S. CMIP-5 models project photovoltaics are a no-regrets investment in Europe irrespective of climate change. *Energy* **171**, 135–148 (2019).
47. Ridley, B., Boland, J. & Lauret, P. Modelling of diffuse solar fraction with multiple predictors. *Renew. Energy* **35**, 478–483 (2010).

## Acknowledgements

The authors would like to thank J. Müller for the code used to construct the hourly GSEE input data from the daily global horizontal solar radiation data.

## Author contributions

M.W., S.P. and B.S. designed the study. B.S., S.P., M.W. and B.v.d.Z. drafted the article. B.S. and S.Y. gathered the data. B.S. analysed the data. B.S. generated the figures. All authors worked on the final manuscript.

## Competing interests

The authors declare no competing interests.

## Additional information

**Supplementary information** is available for this paper at <https://doi.org/10.1038/s41560-019-0412-4>.

**Reprints and permissions information** is available at [www.nature.com/reprints](http://www.nature.com/reprints).

**Correspondence and requests for materials** should be addressed to B.S.

**Publisher's note:** Springer Nature remains neutral with regard to jurisdictional claims in published maps and institutional affiliations.

© The Author(s), under exclusive licence to Springer Nature Limited 2019